Developmental Cell
Article

SUN1 Is Required for Telomere Attachment to Nuclear Envelope and Gametogenesis in Mice

Xu Ding,[1,5] Rener Xu,[1,5,*] Juehua Yu,[1] Tian Xu,[1,2] Yuan Zhuang,[1,3] and Min Han[1,4,*]
[1] Institute of Developmental Biology and Molecular Medicine and School of Life Science, Fudan University, Shanghai 200433, China
[2] Howard Hughes Medical Institute and Department of Genetics, Yale University School of Medicine, New Haven, CT 06536, USA
[3] Department of Immunology, Duke University Medical Center, Durham, NC 27708, USA
[4] Howard Hughes Medical Institute and Department of Molecular, Cellular, and Developmental Biology, University of Colorado, Boulder, CO 80309, USA
[5] These authors contributed equally to this work.
*Correspondence: rener_xu@fudan.edu.cn (R.X.), mhan@colorado.edu (M.H.)
DOI 10.1016/j.devcel.2007.03.018

SUMMARY

Prior to the pairing and recombination between homologous chromosomes during meiosis, telomeres attach to the nuclear envelope and form a transient cluster. However, the protein factors mediating meiotic telomere attachment to the nuclear envelope and the requirement of this attachment for homolog pairing and synapsis have not been determined in animals. Here we show that the inner nuclear membrane protein SUN1 specifically associates with telomeres between the leptotene and diplotene stages during meiotic prophase I. Disruption of *Sun1* in mice prevents telomere attachment to the nuclear envelope, efficient homolog pairing, and synapsis formation in meiosis. Massive apoptotic events are induced in the mutant gonads, leading to the abolishment of both spermatogenesis and oogenesis. This study provides genetic evidence that SUN1-telomere interaction is essential for telomere dynamic movement and is required for efficient homologous chromosome pairing/synapsis during mammalian gametogenesis.

INTRODUCTION

During prophase of meiosis, homologous chromosomes recognize and pair with each other, then synapse along their entire length to facilitate recombination events between them. Prior to pairing, the ends of the chromosomes, telomeres, attach to the nuclear envelope (NE), and then transiently cluster within a limited region of the NE to form a characteristic ''bouquet'' arrangement (Harper et al., 2004; Scherthan, 2001) that is associated with the onset of pairing (Scherthan et al., 1996). After homologous pairing, telomeres disperse from the clustering region and redistribute over the nuclear periphery. Thus, telomere positions undergo dynamic changes during meiotic prophase. Telomere clustering is a widespread phenomenon among eukaryotes and is speculated to facilitate homologous chromosome pairing by positioning the ends of chromosomes in close proximity and promoting alignment between homologs (Harper et al., 2004; Scherthan, 2001). Extensive genetic analyses in both budding and fission yeast have led to the identification of a number of proteins that are involved in telomere clustering (Chikashige et al., 2006; Scherthan, 2006). Although spermatogenesis has been extensively analyzed in animals (Cooke and Saunders, 2002; Russell et al., 1990), studies on the physiological functions of telomere dynamics during meiosis have been limited largely due to the lack of suitable genetic models, and proteins that play critical roles in telomere attachment to the NE have not been identified (Scherthan, 2003). Because missegregation of meiotic chromosomes is a cause of human miscarriage and some developmental defects, study of the mechanisms of chromosome movements during meiosis is of important medical relevance (Hassold and Hunt, 2001).

SUN1 and SUN2 are the first two mammalian SUN proteins identified as homologs of UNC-84, an NE-localized protein required for docking the KASH domain proteins UNC-83 and ANC-1 for nuclear migration and anchorage (Malone et al., 1999; Starr and Han, 2002; Starr et al., 2001). Analyses using tissue culture cells have suggested that the N terminus of both SUN1 and SUN2 localizes inside the nucleoplasm, while the C terminus including the SUN domain is inserted into the perinuclear space between the inner and outer nuclear membranes (Crisp et al., 2006; Haque et al., 2006; Hodzic et al., 2004; Padmakumar et al., 2005). Consistent with results of genetic studies of *unc-84* in *Caenorhabditis elegans*, recent cell-culture studies have indicated that SUN1 and SUN2 are required for the NE anchorage of Syne2/NUANCE/Nesprin-2 (Crisp et al., 2006; Padmakumar et al., 2005). Syne2 is a large KASH domain protein that may act to connect the nucleus to the actin cytoskeleton (Apel et al., 2000; Starr and Han, 2002; Zhang et al., 2005, 2007; Zhen et al., 2002). SUN1 appears to be expressed in multiple tissues in mice (Crisp et al., 2006). However, the physiological functions of SUN1 remain obscure.

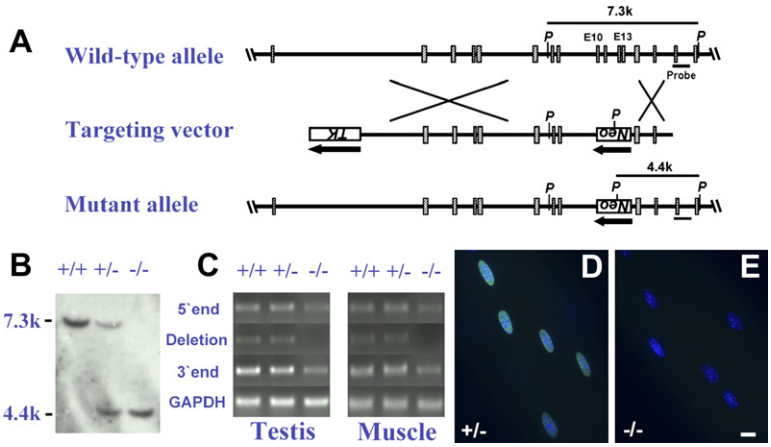

Figure 1. Targeted Disruption of the Mouse *Sun1* Gene

(A) Schematic illustrations of the mouse *Sun1* wild-type allele, targeting vector, and mutant allele. The probe used for Southern blot analysis and sizes of the restriction fragments are indicated. *P*, PvuII.

(B) Southern blot analysis of tail DNA from *Sun1*$^{+/+}$, *Sun1*$^{+/-}$, and *Sun1*$^{-/-}$ mice using the probe indicated in (A). Genomic DNA was digested with PvuII.

(C) RT-PCR of testis and muscle samples using primers specific to *Sun1* cDNA as indicated. GAPDH was used as an internal control.

(D and E) Antibody staining of SUN1 (green) in muscle fibers from adults. Nuclei were stained with DAPI (blue). The scale bar represents 10 μm.

RESULTS

Targeted Disruption of the *Sun1* Gene

We generated SUN1-deficient mice by homologous recombination in embryonic stem (ES) cells. Exons coding all three putative transmembrane domains of SUN1 were replaced by the neomycin resistance cassette (Figure 1A). Three independent targeted ES clones were used to generate chimeric mice, and heterozygous and homozygous mutant progeny were identified by PCR and Southern blot analysis (Figure 1B). RT-PCR was performed to confirm that normal mRNA transcripts were absent in the homozygous *Sun1* targeting mice (Figure 1C). When muscle fibers derived from homozygous mice were analyzed by immunofluorescence with a rabbit polyclonal antibody raised against the coiled-coil domain of SUN1 protein (see Figure S2 in the Supplemental Data available with this article online), we detected SUN1 protein in samples derived from wild-type or heterozygous *Sun1* knockout (*Sun1*$^{+/-}$) mice but not samples from homozygous mutant (*Sun1*$^{-/-}$) mice (Figures 1D and 1E). These results indicate that the targeted mutation mostly likely eliminated *Sun1* function.

Heterozygous *Sun1*$^{+/-}$ mice are normal, and interbreeding of *Sun1*$^{+/-}$ mice yielded a Mendelian distribution of viable *Sun1*$^{+/+}$, *Sun1*$^{+/-}$, and *Sun1*$^{-/-}$ offspring (92:201:96), suggesting that the zygotic *Sun1* gene product is not essential for normal embryonic development.

SUN1 Is Required for Gametogenesis

Both male and female *Sun1*$^{-/-}$ mice developed normally into adults and lived more than 1 year with no obvious difference in general physical appearance compared to their littermates. However, both male and female *Sun1*$^{-/-}$ mice were sterile. The testes of adult *Sun1*$^{-/-}$ males were much smaller than those of *Sun1*$^{+/+}$ or *Sun1*$^{+/-}$ littermates (Figure 2A). Histological examination of testes of *Sun1*$^{-/-}$ males indicated that germ cells were largely depleted in seminiferous tubules (Figures 2B and 2C). More specifically, spermatids and spermatozoa were completely absent and only abnormal spermatocyte-like cells were accumulated in some tubules (Figures 2D–2G). Furthermore, a TUNEL assay revealed many prominent positive signals in *Sun1*$^{-/-}$ seminiferous tubules compared with very few signals in *Sun1*$^{+/-}$ mice (Figures 2I and 2H), indicating the occurrence of massive apoptotic events that likely account for the absence of spermatids and spermatozoa in *Sun1*$^{-/-}$ testes. Consequently, there was no mature sperm in either the caput or cauda epididymal lumen of *Sun1*$^{-/-}$ males (Figures 2J–2M). Further examinations confirmed that spermatogenesis in *Sun1*$^{-/-}$ mice was arrested in meiotic prophase (Figure S1).

SUN1 Colocalizes with Telomeres from Leptotene to Diplotene Stages

Immunofluorescence analysis with the anti-SUN1 antibody could ubiquitously detect specific signals in both somatic and germ cells from wild-type or *Sun1*$^{+/-}$ mice, but no signals in *Sun1*$^{-/-}$ cells (Figures 1D, 1E, and 3A–3F). In somatic cells, such as leydig cells and mouse embryonic fibroblast (MEF) cells, SUN1 distributed evenly around the NE (Figures 3A, 3B, and 3D). SUN1 protein was also abundant in spermatids, and the distribution pattern changed in different developmental stages (Figures 3B and 3G and data not shown). Most strikingly, in primary spermatocytes, SUN1 distributed as foci scattered over the nuclear periphery (Figures 3A and 3B). Such a pattern is similar to the NE localization of telomeres in some stages of primary spermatocytes (Scherthan et al., 1996).

The above results indicated an intriguing role of SUN1 in meiosis and its potential interaction with telomeres. We then simultaneously applied fluorescence in situ hybridization (FISH) analysis of telomeres (Tel-FISH) and SUN1 immunostaining to MEF cells and cryosections of adult testes. In somatic cells, anti-SUN1 signals were distributed all around the NE, while Tel-FISH signals were observed inside the nucleoplasm (Figures 3D–3F). In primary spermatocytes, in which telomeres are attached to the inner nuclear membrane (INM), Tel-FISH signals coincided with those of anti-SUN1, indicating that SUN1 colocalized with telomeres in these cells (Figures 3G–3I). The colocalization was no longer observed in round spermatids. We

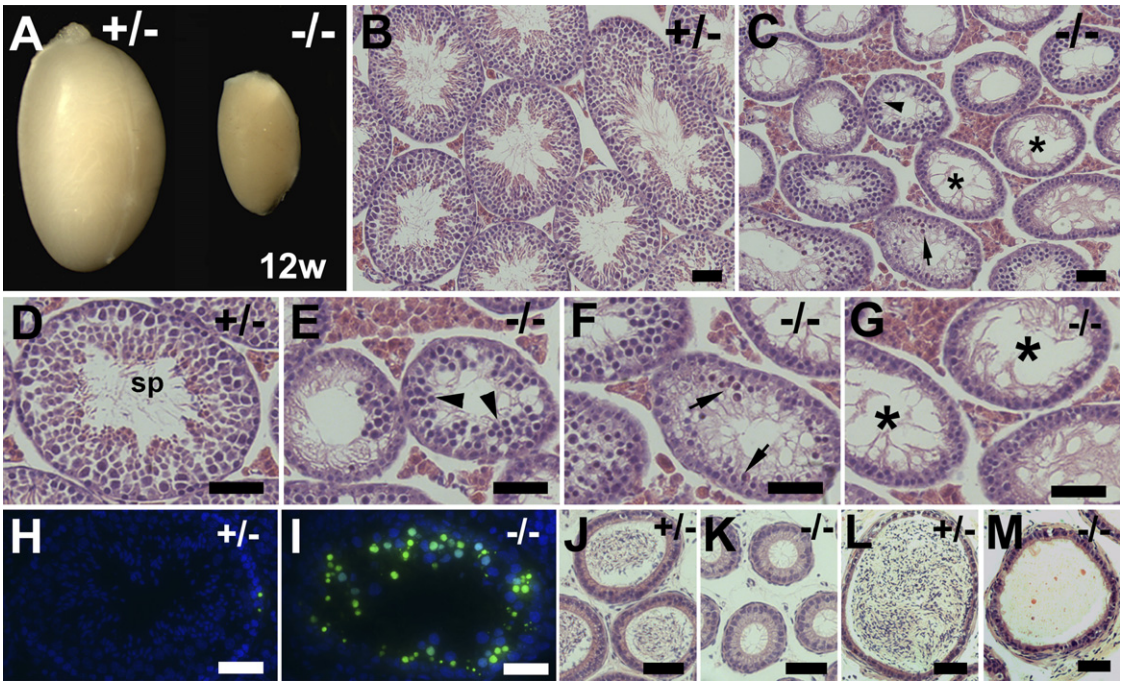

Figure 2. Spermatogenesis Is Disrupted in *Sun1*$^{-/-}$ Mice

(A) Testes from 12-week-old *Sun1*$^{+/-}$ and *Sun1*$^{-/-}$ mice.

(B–G) Hematoxylin and eosin-stained histological cross-sections of testes from adults.

(D–G) Enlarged images of regions in (B) and (C). Arrowheads in (C) and (E) indicate abnormal spermatocyte-like cells in *Sun1*$^{-/-}$ mice. Arrows in (C) and (F) point to hematoxylin-stained pyknotic nuclei indicating apoptotic events. Asterisks in (C) and (G) show vacuolated seminiferous tubules in which both spermatozoa and spermatids are absent.

(H and I) TUNEL-stained cryosections of testes from adult *Sun1*$^{+/-}$ and *Sun1*$^{-/-}$ mice. Many TUNEL-positive cells are observed in *Sun1*$^{-/-}$ testes. Nuclei were stained with DAPI (blue).

(J–M) Caput epididymis (J and K) and cauda epididymis (L and M) from *Sun1*$^{+/-}$ and *Sun1*$^{-/-}$ adults. There is no sperm in the epididymis from *Sun1*$^{-/-}$ mice.

sp, sperm. The scale bars represent 50 μm.

also analyzed the dynamics of SUN1 and telomeres during meiotic prophase by examining the localization of SUN1 and telomeres in testes sections from 8.5 dpp (days postpartum), 10.5 dpp, and 12.5 dpp mice. At these ages, the germ cells from gonia to pachytene stages can easily be identified (Scherthan et al., 1996). We observed that before telomeres attached to the INM, SUN1 foci were distributed evenly around the NE. Later, SUN1 foci aggregated to form larger and fewer dots and became colocalized with telomeres at the NE. Henceforth, SUN1 accompanied telomeres throughout the clustering-dissolution process (Figures 4A–4L; Figure S3). We also analyzed the dynamic distribution of SUN1 during meiotic prophase by coimmunostaining with anti-SYCP3, anti-SYCP1, and anti-SUN1 antibodies in spermatocyte spreads. SYCP3 is one of the lateral elements of the synaptonemal complex (SC) and has been used to mark both paired and unpaired chromosome regions (Lammers et al., 1994). SYCP1 is a major component of the transverse filaments of the SC and has been used to mark the synapsed regions of chromosomes (Meuwissen et al., 1992). SUN1 signal was visible at the chromosome ends in early leptotene stage through diplotene stage, including the homolog pairing, synapsis, and desynapsis processes (Figures 4M–4P). The absence of the anti-SUN1 spots at diakinesis stage suggests that SUN1 is detached from the telomeres at that stage (Figure 4Q). These results are consistent with the dynamic behavior of telomere-NE attachment/detachment during meiotic prophase (Scherthan, 2001).

Telomere NE Attachment Is Disrupted in *Sun1*$^{-/-}$ Mice

The colocalization of SUN1 and telomeres at the NE during meiotic prophase suggested the possibility that SUN1 anchors telomeres to the INM. This hypothesis was strongly supported by Tel-FISH analysis of testes sections of *Sun1*$^{-/-}$ mice. Judging from the results of anti-SYCP3 staining of 18.5 dpp *Sun1*$^{+/+}$ or *Sun1*$^{+/-}$ testes sections, most (90.8%; Table S1A) of the spermatocytes from the first wave of spermatogenesis had reached the pachytene stage, at which telomeres had inserted into the NE marked by anti-LaminB staining (Figure 5A) (Moss et al., 1993). In contrast, nearly all cells (96.2%; Table S1B) in *Sun1*$^{-/-}$ littermates displayed a zygotene-like SYCP3 staining pattern, and the telomeres localized

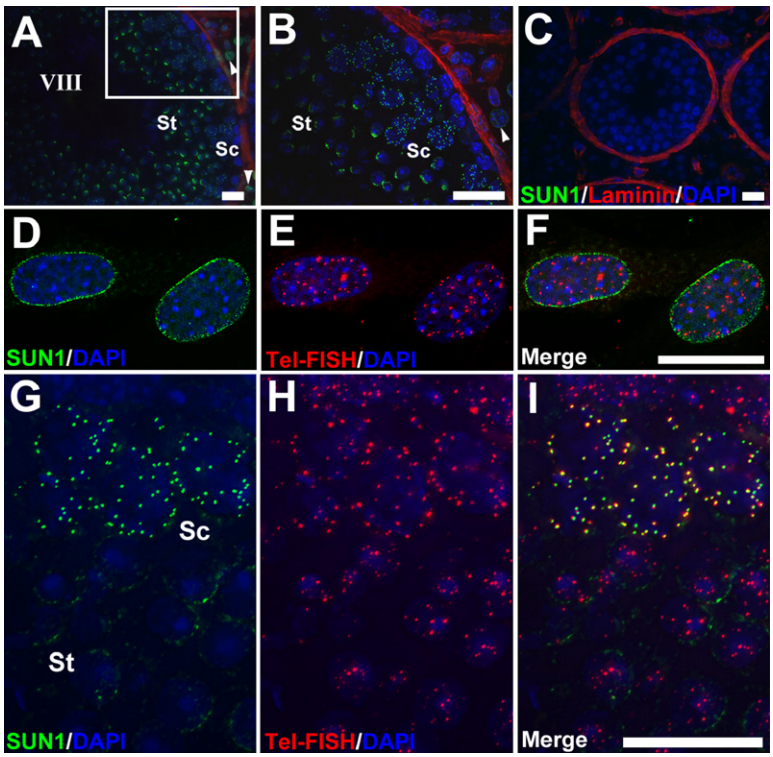

Figure 3. Distribution Pattern of SUN1 in Somatic and Germ Cells

(A–C) Fluorescent images (projections of Z stacks) of seminiferous tubules from *Sun1*$^{+/-}$ ([A and B], at stage VIII) and *Sun1*$^{-/-}$ (C) adult mice stained with anti-SUN1, and counterstained with anti-Laminin to mark the basal lamina of seminiferous tubules. (B) shows a higher-magnification image of the framed section in (A). Arrowheads indicate an NE localization of SUN1 in leydig cells. In spermatids (St), SUN1 is also highly expressed. In (B), the punctate SUN1 signals are scattered over the nuclear periphery in primary spermatocytes (Sc).

(D–F) Single-layer images showing telomeres (red) and anti-SUN1 (green) staining in wild-type mouse embryonic fibroblast (MEF) cells. SUN1 is distributed all around the NE, while telomeres are located inside the nucleoplasm of MEFs.

(G–I) Fluorescent images (projections of Z stacks) showing that the anti-SUN1 antibody signals (green in [G]) and the telomere FISH signals (red in [H]) are colocalized (yellow in [I]) in spermatocytes (Sc) but not in spermatids (St). Nuclei were stained with DAPI (blue). The scale bars represent 20 μm.

predominantly inside the nucleoplasm (Figure 5B), indicating that SUN1 is required for the docking of telomeres at the NE. We also examined the distribution of telomeres in the *Sun1*$^{-/-}$ spermatocytes of 12.5 dpp and 15.5 dpp juveniles as well as adult mice, and never observed normal NE attachment and clustering of telomeres (data not shown). These results strongly support a conclusion that the INM protein SUN1 is required for telomere attachment to the NE in primary spermatocytes. Our analysis also indicated that the associations of TRF1 and Rap1, two known telomere-binding proteins, with the telomeres were not disrupted in *Sun1*$^{-/-}$ mutants (Figure S4).

Efficient Homologous Chromosome Pairing, Synapsis, and Recombination Are Severely Impaired in *Sun1*$^{-/-}$ Spermatocytes

Sun1$^{-/-}$ mice thus provided an animal model devoid of telomere attachment and clustering, suitable to investigate the function of these cellular processes in mammals. To determine whether SUN1 is essential for homologous chromosome synapsis, we quantified the extent of synapsis in spermatocytes undergoing the first wave of spermatogenesis, which are approximately synchronized. From 18.5 dpp mice testes, 90.8% of the *Sun1*$^{+/-}$ spermatocytes (n = 2249) were at pachytene stage, at which all chromosomes are fully synapsed with their partners except the partial synapsis between X and Y chromosomes (Table S1A). However, none of the *Sun1*$^{-/-}$ spermatocytes showed normal homologous pairing and synapsis (n = 1785). In addition, less than 1% of the *Sun1*$^{-/-}$ spermatocytes contained more than ten partially or fully synapsed chromosomes (Table S1B), indicating that synapsis was severely impaired in mutant spermatocytes. This is further supported by analyzing the frequency of the numbers of synapsed chromosomes in individual spermatocyte spreads from adults (Figure S5).

To determine whether the remaining synapsis observed in *Sun1*$^{-/-}$ spermatocytes was between homologous chromosomes, we monitored the pairing of individual chromosomes by applying chromosome painting to spermatocyte spreads. Consistent with the severe defects in overall chromosome pairing, the frequencies of pairing of chromosomes 8 and 19 were dramatically reduced (Figures 5C–5G). However, nonhomologous pairing involving chromosomes 8 or 19 was not detected in mutant spermatocytes, indicating that the mechanism for homolog recognition and for the prevention of pairing between nonhomologs is still functional in the mutant. Among the paired chromosomes 8 and 19, we found that the percentage of homologs with partial synapsis was dramatically increased in the mutants (Figure 5H), suggesting that telomere attachment to the NE and chromosomal bouquet formation may also be required for the process of extending short synapsed regions to full-length SCs. Given the recent finding that telomere attachment to the NE was dependent on functional telomere repeats which localize to attachment plates (Liebe et al., 2004; Liu et al., 2004), our result is consistent with the previous observation that shortened telomeres and lack of perinuclear distribution of telomeres in G4 *TR*$^{-/-}$ meiocytes contribute to impaired assembly of SCs (Liu et al., 2004).

Recent work has indicated that, in mouse, the initiation of synapsis depends on the occurrence of programmed double-strand breaks (DSB) in the genome and the

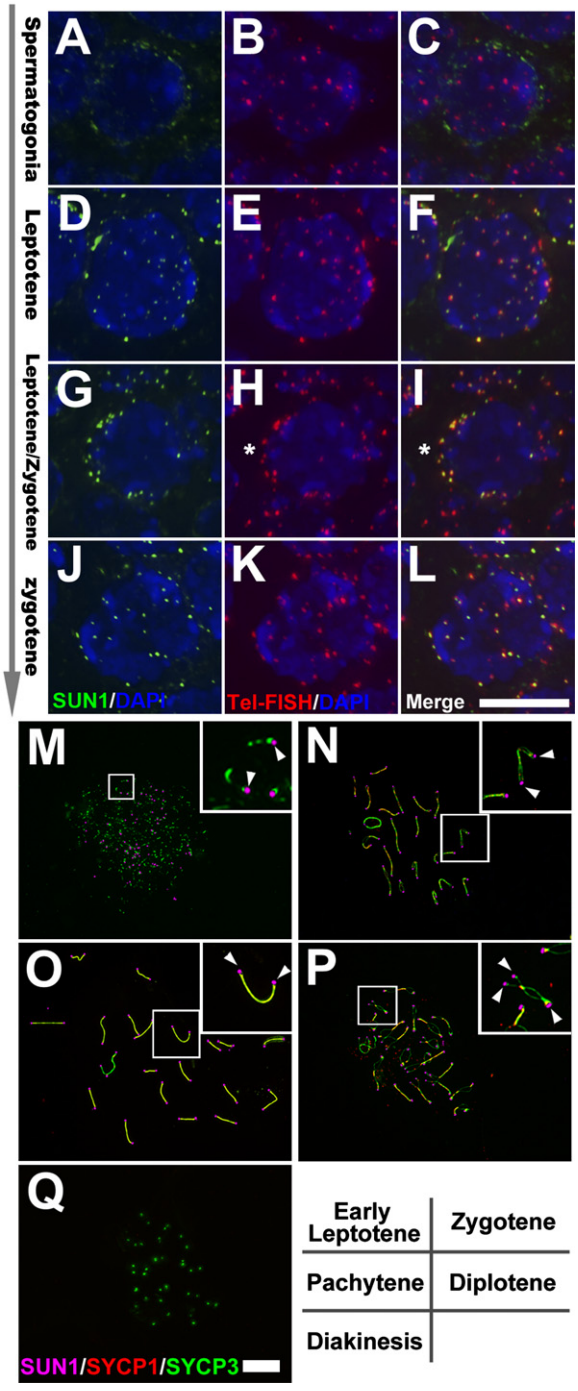

Figure 4. Dynamics of SUN1-Telomere Interaction during Meiotic Prophase

(A–L) Dynamics of SUN1 and telomere colocalization during meiotic prophase I. Anti-SUN1, telomere FISH, and merged images (projections of Z stacks) at spermatogonial (A–C), leptotene (D–F), leptotene-to-zygotene (G–I), and zygotene (J–L) stages are shown. Colocalization of SUN1 and telomeres occurred after telomere NE attachment during the leptotene stage. Asterisks in (H) and (I) indicate the clustering of telomeres. Nuclei were stained with DAPI (blue).

(M–Q) Merged images of anti-SUN1, anti-SYCP3, and anti-SYCP1 at early leptotene (M), zygotene (N), pachytene (O), diplotene (P), and diakinesis (Q) stages in spermatocyte spreads. SUN1 resides at both ends of the chromosomes before diakinesis. Examples of SUN1 localization at different stages (small frames in [M]–[P]) were enlarged in the insets. Arrowheads point to the SUN1 signals associated with the ends of chromosomes.

The scale bars represent 10 μm.

initiation of their repair (Gerton and Hawley, 2005; Zickler, 2006). Because synapsis is severely impaired in *Sun1*$^{-/-}$ mutants, we examined the potential defects in DSB formation and the subsequent development of reciprocal exchanges (crossovers) between homologous chromosomes by staining using anti-RAD51 and anti-MLH1 antibodies, respectively. RAD51 is a DSB repair protein and is involved in earlier steps of meiotic recombination (Moens et al., 1998, 2002), whereas MLH1 marks the sites of crossovers (Anderson et al., 1999; Moens et al., 2002). Our statistical data showed that in both wild-type and *Sun1*$^{-/-}$ spermatocytes, the RAD51 foci were detectable at the leptotene stage and the foci numbers reached the maximum at the leptotene/zygotene-like stage (Figures 5I and 5J; Table S3) (Barlow et al., 1997; Moens et al., 1997). The maximal foci numbers were 240 in *Sun1*$^{-/-}$ cells and 235 in wild-type. However, in 48% of zygotene-like *Sun1*$^{-/-}$ spermatocytes (n = 406), compared to 3% of wild-type spermatocytes (n = 173), numerous ($81 \leq n \leq 240$) RAD51 foci were observed, indicating that the RAD51 foci failed to be efficiently eliminated in *Sun1*$^{-/-}$ cells (Table S3). The MLH1 foci, normally detected in wild-type pachynema, were not found in *Sun1*$^{-/-}$ meiotic cells (Figures 5K and 5L), suggesting the failure of the development of crossovers. These observations indicate that in *Sun1*$^{-/-}$ spermatocytes, pairing and synapsis can be initiated following the formation of DSBs, but the progression and completion of pairing, synapsis, and recombination are seriously hampered by the disruption of telomere attachment and formation of the chromosomal bouquet in the mutant mice. The defective synapsis and recombination in the *Sun1*$^{-/-}$ mice are similar to, but more severe than, those reported in G4 *TR*$^{-/-}$ mice (Liu et al., 2004).

Homologous Synapsis during Oogenesis Is Also Impaired in *Sun1*$^{-/-}$ Mice

Previous studies suggest that oogenesis in mammals is more tolerant of meiotic defects. Mutations which lead to meiotic defects in spermatogenesis frequently escape meiotic failure during oogenesis (Hunt and Hassold, 2002; Kolas et al., 2005). We thus further analyzed oogenesis in *Sun1*$^{-/-}$ mice. We observed that in adult *Sun1*$^{-/-}$ females, the ovaries were also much smaller than those of their littermates (data not shown), and that the oocytes and ovarian follicles were completely absent (Figures 6A and 6B). Furthermore, there are no oocytes detected in day 5 neonatal *Sun1*$^{-/-}$ ovaries (Figures 6C and 6D). A TUNEL assay showed that there were dramatically increased positive signals in the ovaries of *Sun1*$^{-/-}$ E17.5 embryos compared to *Sun1*$^{+/-}$ ovaries (Figures 6E and 6F). Tel-FISH analysis combined with anti-SUN1

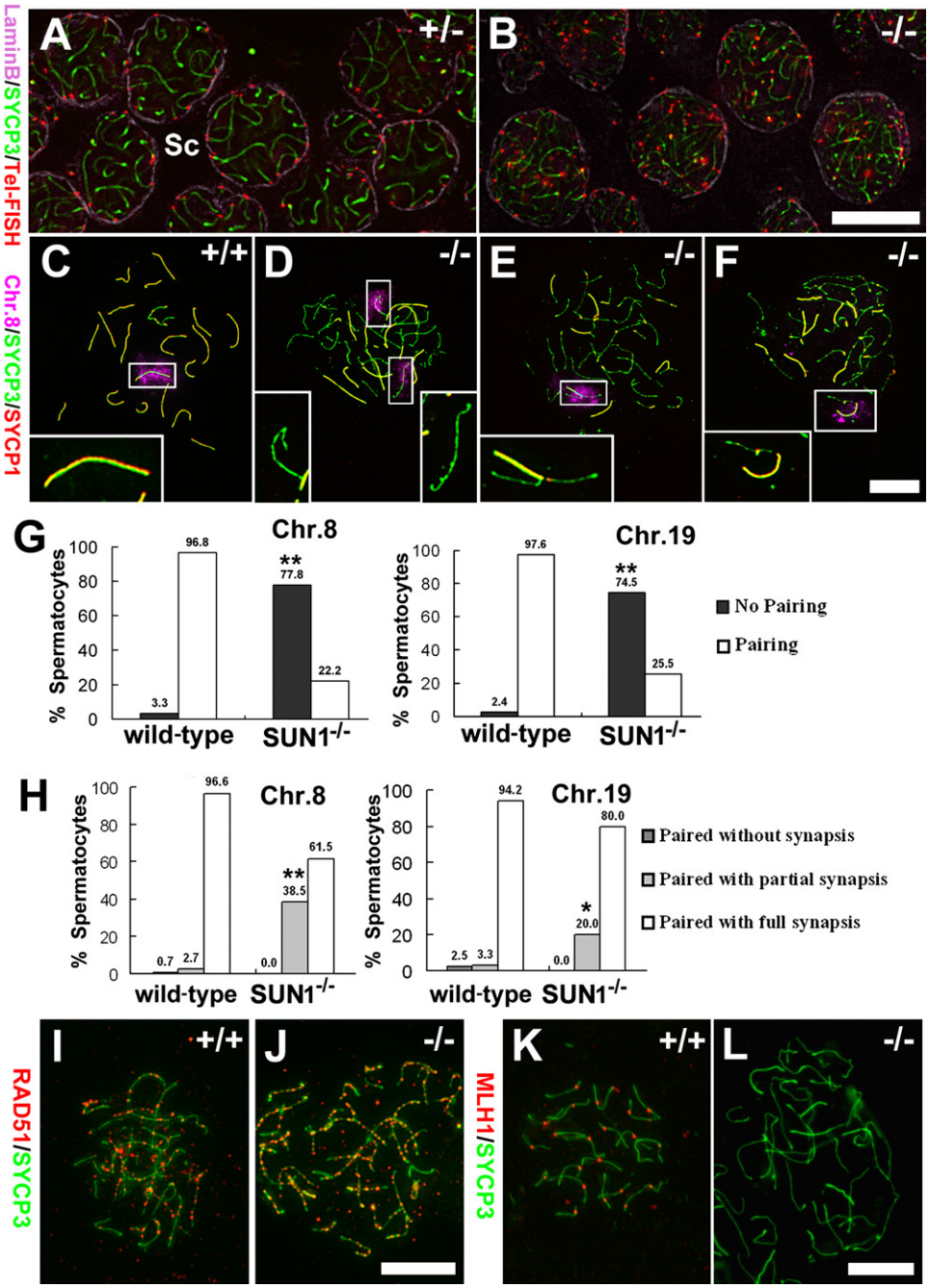

Figure 5. Telomere Attachment to the NE and Homologous Chromosome Pairing/Synapsis Formation Are Severely Impaired in *Sun1*$^{-/-}$ Mice

(A and B) Single-layer images showing telomere (red), anti-SYCP3 (green), and anti-LaminB (purple) staining in sections of testes from 18.5 dpp mice. Telomeres are attached to the NE in *Sun1*$^{+/-}$ spermatocytes (A), but not in *Sun1*$^{-/-}$ spermatocytes (B).

(C–F) Fluorescent images of spermatocyte spreads simultaneously labeled with anti-SYCP1 (red), anti-SYCP3 (green), and chromosome 8 painting (purple). Synapsis formation, indicated by anti-SYCP1 staining, is severely reduced in *Sun1*$^{-/-}$ spermatocytes, consistent with the drastic increase in the number of chromosomes that are marked by anti-SYCP3. Chromosome 8 axes were embedded in the FISH painting signals. Insets are enlarged figures showing SYCP1/SYCP3 staining alone of the framed regions. The insets in (C) and (F) show fully synapsed chromosome 8. (D) and (E) show unpaired and partially synapsed chromosome 8, respectively. The images for chromosome 19 are similar (not shown).

(G) Pairing frequencies of chromosomes 8 and 19 in wild-type (n = 154 and 124, respectively) and *Sun1*$^{-/-}$ (n = 117 and 157, respectively) primary spermatocytes.

(H) Frequencies of synapsis formation of paired chromosomes 8 and 19 in wild-type (n = 149 and 121, respectively) and *Sun1*$^{-/-}$ (n = 26 and 40, respectively) primary spermatocytes. Because the synapsed bivalents begin to desynapse and separate from the diplotene stage, the wild-type diplotene and diakinesis spermatocytes are not included in the statistics (G and H).

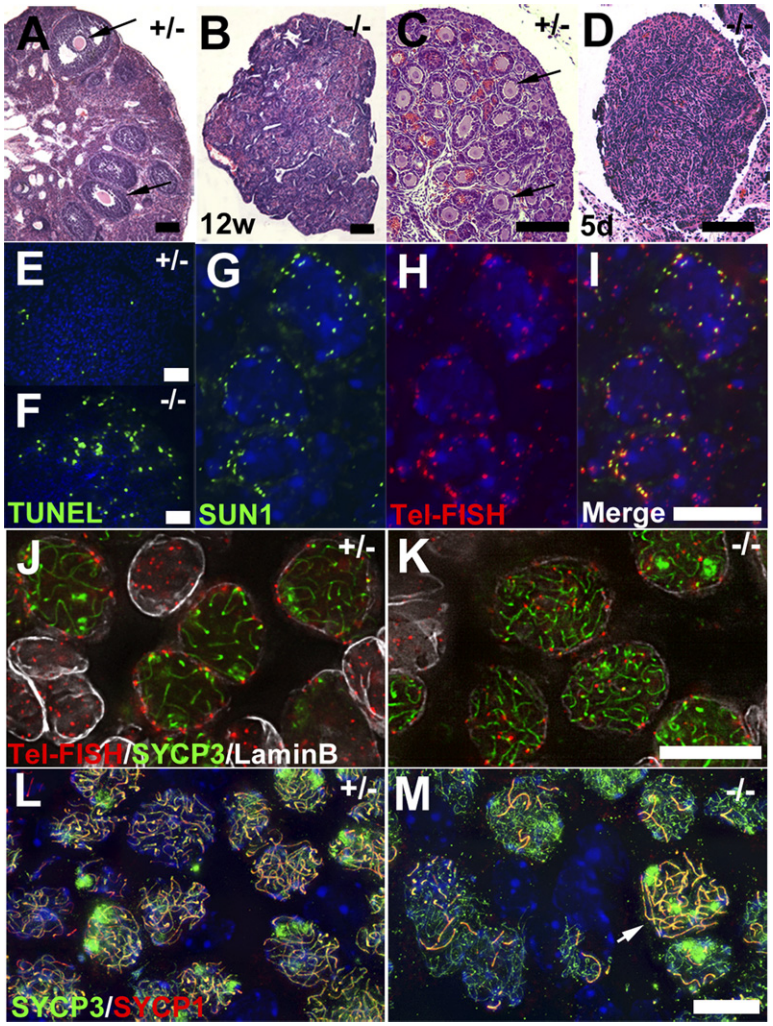

Figure 6. Oogenesis Is Blocked in *Sun1*$^{-/-}$ Females

(A–D) Hematoxylin and eosin-stained histological cross-sections of ovaries in 12-week-old and 5 dpp females. Arrows in (A) and (C) indicate oocytes and growing follicles that are not detected in *Sun1*$^{-/-}$ ovaries (B and D).

(E and F) TUNEL-stained cryosections of ovaries from E17.5 embryos. Many TUNEL-positive cells are detected in the *Sun1*$^{-/-}$ ovary compared to that in the *Sun1*$^{+/-}$ ovary, indicating a dramatic increase in apoptotic events in the mutants.

(G–I) Anti-SUN1 (green in [G]), telomere FISH (red in [H]), and merged (yellow in [I]) immunofluorescent images (projections of Z stacks) of ovary cryosections from E17.5 embryos. SUN1 is colocalized with telomeres in primary oocytes.

(J and K) Single-layer images showing telomere (red), anti-SYCP3 (green), and anti-LaminB (white) staining in sections of ovary from E17.5 embryos. Telomeres are attached to the NE in *Sun1*$^{+/-}$ oocytes (J), but not in *Sun1*$^{-/-}$oocytes (K).

(L and M) Merged immunofluorescent images (projections of Z stacks) of ovary sections from E17.5 embryos stained with anti-SYCP3, anti-SYCP1, and DAPI. The arrow in (M) indicates a very rare normal-looking synapsed oocyte (0.1%, n = 880).

Nuclei were stained with DAPI (blue) (E–I, L, and M). The scale bars in (A)–(F) represent 50 μm, in (G)–(M), 10 μm.

immunostaining on cryosectioned ovaries from wild-type E17.5 embryos indicated that SUN1 colocalized with telomeres in oocytes (Figures 6G–6I). As in spermatocytes, telomere attachment to the NE was also disrupted in *Sun1*$^{-/-}$ oocytes (Figures 6J and 6K). We also investigated pairing and synapsis processes in E17.5 ovaries by colabeling with anti-SYCP3 and anti-SYCP1 antibodies. At E17.5, 90.5% (n = 737) *Sun1*$^{+/-}$ oocytes reached pachytene stage, with all homologous chromosomes synapsed and coated with both SYCP3 and SYCP1 (Figure 6L; Table S2A). Similar to the situation in males, chromosomes from *Sun1*$^{-/-}$ E17.5 oocytes were normally coated by SYCP3, but the number of chromosomes was much higher than that of the control, which was accompanied by a severe reduction in synapsed chromosomes marked with SYCP1 (Figure 6M; Table S2). Only very rare oocytes (0.1%, n = 880) showed a pachytene-like synapsis.

These results indicate that SUN1 plays a critical role in anchoring telomeres at the NE for telomere clustering, which is required for proper homologous chromosome pairing and synapsis formation during both spermatogenesis and oogenesis in mammals. The depletion of gametes in mutant mice is likely the consequence of massive apoptotic events that are trigged by the failure of SC formation (Handel, 1998; Roeder and Bailis, 2000).

DISCUSSION

To our knowledge, the *Sun1*$^{-/-}$ mouse is the first genetic model to provide functional insight into telomere NE attachment during meiosis in mammals. The results

(I and J) Fluorescent images of spermatocyte spreads simultaneously labeled with anti-RAD51 (red) and anti-SYCP3 (green). Rad51 foci located to both the wild-type (I) and *Sun1*$^{-/-}$ (J) chromosomes.

(K and L) Fluorescent images of spermatocyte spreads simultaneously labeled with anti-MLH1 (red) and anti-SYCP3 (green). There are no MLH1 foci located to *Sun1*$^{-/-}$ (L) chromosomes as in wild-type (K).

The scale bars represent 10 μm. (Contingency tables and chi-square; *p = 0.0016; **p < 0.0001.)

described here are comparable to those from studies in the yeast *Saccharomyces cerevisiae*, where defects in chromosome synapsis, recombination, and segregation are associated with mutations in the meiosis-specific telomeric protein Ndj1 that disrupts the attachment of telomeres to the NE (Conrad et al., 1997; Wu and Burgess, 2006). It is not clear at this point how SUN1 interacts with telomeres. A recent study in the yeast *S. pombe* has shown that a protein complex containing Bqt1 and Bqt2 mediates the interaction between Sad1 and the telomere complex (Chikashige et al., 2006). However, the significant differences between *S. pombe* and animal meiosis suggest that the mechanisms by which SUN proteins interact with telomeres may be different. For example, *S. pombe* does not have the typical synapsis formation seen in animal cells during meiosis and its nucleus has the unique "horsetail" movement which plays a role in meiotic pairing and recombination (Gerton and Hawley, 2005). Furthermore, the N-terminal sequences of Sad1 and SUN1 are very diverse, and we failed to identify mammalian homologs of Bqt1 and Bqt2. It is possible that one or more unknown meiosis-specific proteins mediate the interaction between SUN1 and telomeres. On the other hand, the possibility of a direct interaction between SUN1 and chromatin may not be excluded, particularly as the SUN1 N terminus contains a zinc-finger domain (Padmakumar et al., 2005).

Telomere attachment to the NE is followed by telomere clustering. During the transition, SUN1-telomere pairs move along the NE surface from a dispersed position to sites near the centrosome. The driving force behind such movement in mammals is not known. Previous studies found that, in mammals, telomere attachment to the NE involves filaments spanning the NE and emanating into the cytoplasm (Liebe et al., 2004). SUN1 could be a critical component of these elements. In animals, SUN proteins are known to interact and anchor KASH domain-containing proteins that are proposed to localize at the outer nuclear membrane (Crisp et al., 2006; Haque et al., 2006; Malone et al., 2003; McGee et al., 2006; Padmakumar et al., 2005; Starr and Han, 2002; Starr et al., 2001). As Syne/ANC-1/MSP-300 family proteins are thought to connect the NE to the actin cytoskeleton (Starr and Fischer, 2005; Yu et al., 2006; Zhang et al., 2007), the possibility that one of the three known mammalian KASH proteins is involved in linking SUN1 to the cytoskeletal system remains to be investigated.

Although SUN1 is widely expressed in many somatic tissues, we did not detect any telomeric dysfunction in *Sun1*$^{-/-}$ somatic cells. Simultaneous SUN1 immunostaining and Tel-FISH on both the mitotic cells in tissue sections and cultured MEF cells showed that SUN1 did not colocalize with telomeres (Figure S4) and that there was also no abnormality in proliferation of MEF cells from *Sun1*$^{-/-}$ mice (data not shown). *Sun1*$^{-/-}$ mice also developed normally and were healthy. These results are consistent with those that SUN1 is not essential for normal telomeric functions in somatic cells. However, genetic analysis of SUN proteins in *C. elegans* (Malone et al., 1999, 2003; Starr and Han, 2002; Starr et al., 2001) indicated that they interact with KASH domain proteins for important cellular functions in somatic cells. Supporting the proposed functions of SUN proteins in somatic cells, studies in tissue culture cells also indicate that SUN1 interacts with nuclear lamin and KASH domain proteins (Crisp et al., 2006; Haque et al., 2006; Padmakumar et al., 2005). In mammals, SUN2 shares similar protein structure with SUN1, and both show ubiquitous gene expression profiling in mouse and human in microarray analyses (http://symatlas.gnf.org/SymAtlas/). Recent studies demonstrated that both SUN1 and SUN2 contribute to Syne2 NE anchorage in somatic cells (Crisp et al., 2006). These findings hint at the redundant roles of SUN1 and SUN2 in somatic cells. SUN2 was not found to express in meiotic cells (data not shown), which might be a reason why there is no redundancy associated with SUN1 function in telomere attachment to the NE.

In summary, our results reveal that the inner nuclear membrane protein SUN1 is required for telomere attachment to the nuclear envelope during meiotic prophase I and demonstrate that telomere attachment to the NE is essential for the efficient pairing/synapsis of homologous chromosomes and gametogenesis in mammals.

EXPERIMENTAL PROCEDURES

Generation of SUN1-Deficient Mice

Genomic DNA fragments from an Sv129 strain BAC clone (538A12, Invitrogen) were used to construct the *Sun1* gene targeting vector. The 1.8 kb fragment containing exon 14 and exon 15 was PCR amplified from the DNA derived from the BAC clone with primer pair prDX077/prDX078 (see primer list in Supplemental Data). After sequencing verification, this fragment was inserted into the XhoI site of the pPNT vector as the short arm. For the long arm, an 11.5 kb EcoRI fragment within the *Sun1* gene obtained from the above BAC DNA was ligated into the EcoRI site of the short arm-containing pPNT plasmid.

The linearized *Sun1* targeting vector was electroporated into W4/129S6 ES cells. After double selection, ES cell clones were screened by PCR (primer pair prDX100/prDX101) and confirmed by Southern blot analysis. Three targeted ES clones were injected into C57BL/6J blastocysts and the status of the targeted *Sun1* allele in mice was confirmed by both PCR and Southern blot analysis. Because *Sun1*$^{-/-}$ mice from three independent ES lines displayed the same phenotypes, one line was used in further studies.

RT-PCR

Total mRNAs were isolated from the tibialis anterior muscles or testes of adult mice using TRIzol reagent (Invitrogen). cDNAs were produced using an RNA PCR kit (TAKARA) following the manufacturer's instructions. Three primer pairs prDX177/prDX178, prDX142/prDX143, and prDX140/prDX141 were used, respectively, to amplify the coding regions located upstream, within, and downstream of the deletion in the targeted allele. Glyceraldehyde-3-phosphate dehydrogenase (GAPDH) served as an internal control.

Generation of Anti-SUN1 Antibody

The DNA fragment coding for 171 amino acids of the SUN1 coiled-coil domain was PCR amplified from the DNA derived from the *Sun1* cDNA clone (8571051, ATCC) with primers prDX055 and prDX056, and then cloned into pET28 (Novagen) for standard protein expression and purification. Polyclonal antibodies were raised by immunizing rabbits with the purified fusion proteins and were affinity purified with Hitrap NHS-activated HP columns (Amersham Biosciences). Some affinity-purified

antibodies were further labeled with biotin using a protein labeling kit (AnaTag).

Histological Analysis

Frozen sections: after the animals were exterminated by cervical dislocation, tissues of interest were dissected out and embedded in OCT. Samples were then quickly frozen in liquid nitrogen-cooled isopentane, and 8 μm slices were collected. Paraffin sections: adult mice were anaesthetized and perfused with 3.7% formaldehyde in PBS (pH 7.4). Tissues were postfixed with the same fixative and processed for paraffin embedding and sectioning at 5 μm. Sections were stained with hematoxylin and eosin. TUNEL assays were performed following a protocol described previously (Tornusciolo et al., 1995).

Spermatocyte Spreading

Detergent spreading of spermatocytes was performed as described in Scherthan et al. (2000).

Immunofluorescence Staining, Telomere FISH, Chromosome Painting, and Microscopy

Immunofluorescence was carried out following a protocol described previously (Scherthan et al., 2000). Primary antibodies used were rabbit anti-SUN1 (1:40), rabbit anti-SYCP3 (1:500; a gift from Norio Nakatsuji), goat anti-SYCP3 (1:400; a gift from Terry Ashley), rabbit anti-SYCP1 (1:400; Novus Biologicals), rabbit anti-Laminin (1:300; Sigma), goat anti-LaminB (1:100; Santa Cruz Biotechnology), anti-RAD51 (1:30; H-92, Santa Cruz Biotechnology), and MLH1 (1:30; G168-15, Abcam). Secondary antibodies were goat anti-rabbit IgG-FITC (Sigma), goat anti-rabbit IgG-TRITC (Sigma), and horse anti-mouse IgG-biotin (Vector Labs). When SUN1, SYCP1, and SYCP3 were visualized simultaneously, SYCP1 and SYCP3 were first visualized consecutively. The preparations were then fixed in a 1% formaldehyde/1× PBS solution for 1 min followed by incubation with the biotin-labeled antibodies against SUN1 and detection with streptavidin-Cy5 (Zymed).

Combinatorial immunostaining and telomere FISH were carried out following the protocol described in Scherthan et al. (2000) with minor modifications. Briefly, SUN1 or LaminB was first immunostained as described above, except that biotinylated goat anti-rabbit (1:400; Vector Labs) or biotinylated bovine anti-goat antibody (1:200; Santa Cruz Biotechnology) was used as the secondary antibody. Slices were then thoroughly washed with PBS at room temperature and denatured at 85°C for 5 min in the presence of digoxigenin-labeled $(CCCTAA)_7$ oligo probes (Scherthan et al., 1996). Hybridization was then carried out at 37°C for 12 hr. After thoroughly washing in 0.05× SSC at 37°C, signals were detected by staining with anti-digoxigenin rhodamine (Roche Diagnostics) or streptavidin-FITC (Roche Diagnostics). In some cases, SYCP3 was counterstained and visualized by Cy5-conjugated goat anti-rabbit antibody (CHEMICON). Preparations were finally counterstained with DAPI (0.3 μg/ml) and embedded in mounting medium (Vector Shield).

Chromosome painting was carried out on spermatocyte spreads prepared as described above. Slides were denatured at 85°C for 10 min in the presence of biotin-labeled mouse chromosome 8 or 19 paint probes (ID Labs) and hybridized for 72 hr at 37°C. Preparations were then washed by incubating sequentially in 50% formamide/0.5× SSC (twice) and 1× SSC (twice) at 42°C for 5 min each time. After the preparations were colabeled by staining with anti-SYCP1 and anti-SYCP3 antibodies as described above, they were treated with streptavidin-Cy5 for visualizing the chromosome painting results. Preparations were finally counterstained with DAPI (0.3 μg/ml) and embedded in mounting medium (Vector Shield). For unpaired homologs, two distinct chromosomal axial cores, visualized by anti-SYCP3 staining, were associated with two separate FISH painting signals. In contrast, the paired chromosome cores were surrounded by the single FISH signal in one cell. The synapsis formation was further judged by the SYCP1/SYCP3 signals.

Photographs were taken by either a Leica DM RXA2 or DM IRE2 system equipped with A, GFP, N21, TX2, and Cy5 filters and recorded by a Leica DC350F or DFC300 CCD camera. Three-dimensional deconvolution on 0.2 μm spaced image stacks was carried out by Leica Deblur software. Images were manipulated with Leica FW4000 and Adobe Photoshop software.

Supplemental Data

Supplemental Data include five figures and three tables and are available at http://www.developmentalcell.com/cgi/content/full/12/6/863/DC1/.

ACKNOWLEDGMENTS

We are grateful to Yanling Yang, Yanfen Tan, Xiaochang Zhang, Muyun Chen, and Kai Lei for their contributions to the project, Xiaohui Wu, Beibei Ying, Kejing Deng, Ling Sun, and Wufan Tao for help in multiple aspects of this work, Norio Nakatsuji, Terry Ashley, Christa Heyting, Sue Shackleton, Harry Scherthan, Stephen West, Madalena Tarsounas, and Huiling Xu for antibodies and protocols, Aileen Sewell, Jen Blanchette, and Emylie Seamen for comments on the manuscript, and members of the Institute of Developmental Biology and Molecular Medicine for various input. This work is supported by grants from the National Natural Science Foundation, Ministry of Education of China, Ministry of Science and Technology of China, and the Shanghai Municipal Government.

Received: December 14, 2006
Revised: February 22, 2007
Accepted: March 23, 2007
Published: June 4, 2007

REFERENCES

Anderson, L.K., Reeves, A., Webb, L.M., and Ashley, T. (1999). Distribution of crossing over on mouse synaptonemal complexes using immunofluorescent localization of MLH1 protein. Genetics *151*, 1569–1579.

Apel, E.D., Lewis, R.M., Grady, R.M., and Sanes, J.R. (2000). Syne-1, a dystrophin- and Klarsicht-related protein associated with synaptic nuclei at the neuromuscular junction. J. Biol. Chem. *275*, 31986–31995.

Barlow, A.L., Benson, F.E., West, S.C., and Hulten, M.A. (1997). Distribution of the Rad51 recombinase in human and mouse spermatocytes. EMBO J. *16*, 5207–5215.

Chikashige, Y., Tsutsumi, C., Yamane, M., Okamasa, K., Haraguchi, T., and Hiraoka, Y. (2006). Meiotic proteins Bqt1 and Bqt2 tether telomeres to form the bouquet arrangement of chromosomes. Cell *125*, 59–69.

Conrad, M.N., Dominguez, A.M., and Dresser, M.E. (1997). Ndj1p, a meiotic telomere protein required for normal chromosome synapsis and segregation in yeast. Science *276*, 1252–1255.

Cooke, H.J., and Saunders, P.T. (2002). Mouse models of male infertility. Nat. Rev. Genet. *3*, 790–801.

Crisp, M., Liu, Q., Roux, K., Rattner, J.B., Shanahan, C., Burke, B., Stahl, P.D., and Hodzic, D. (2006). Coupling of the nucleus and cytoplasm: role of the LINC complex. J. Cell Biol. *172*, 41–53.

Gerton, J.L., and Hawley, R.S. (2005). Homologous chromosome interactions in meiosis: diversity amidst conservation. Nat. Rev. Genet. *6*, 477–487.

Handel, M.A. (1998). Monitoring meiosis in gametogenesis. Theriogenology *49*, 423–430.

Haque, F., Lloyd, D.J., Smallwood, D.T., Dent, C.L., Shanahan, C.M., Fry, A.M., Trembath, R.C., and Shackleton, S. (2006). SUN1 interacts with nuclear lamin A and cytoplasmic nesprins to provide a physical

connection between the nuclear lamina and the cytoskeleton. Mol. Cell. Biol. *26*, 3738–3751.

Harper, L., Golubovskaya, I., and Cande, W.Z. (2004). A bouquet of chromosomes. J. Cell Sci. *117*, 4025–4032.

Hassold, T., and Hunt, P. (2001). To err (meiotically) is human: the genesis of human aneuploidy. Nat. Rev. Genet. *2*, 280–291.

Hodzic, D.M., Yeater, D.B., Bengtsson, L., Otto, H., and Stahl, P.D. (2004). Sun2 is a novel mammalian inner nuclear membrane protein. J. Biol. Chem. *279*, 25805–25812.

Hunt, P.A., and Hassold, T.J. (2002). Sex matters in meiosis. Science *296*, 2181–2183.

Kolas, N.K., Marcon, E., Crackower, M.A., Hoog, C., Penninger, J.M., Spyropoulos, B., and Moens, P.B. (2005). Mutant meiotic chromosome core components in mice can cause apparent sexual dimorphic endpoints at prophase or X-Y defective male-specific sterility. Chromosoma *114*, 92–102.

Lammers, J.H., Offenberg, H.H., van Aalderen, M., Vink, A.C., Dietrich, A.J., and Heyting, C. (1994). The gene encoding a major component of the lateral elements of synaptonemal complexes of the rat is related to X-linked lymphocyte-regulated genes. Mol. Cell. Biol. *14*, 1137–1146.

Liebe, B., Alsheimer, M., Hoog, C., Benavente, R., and Scherthan, H. (2004). Telomere attachment, meiotic chromosome condensation, pairing, and bouquet stage duration are modified in spermatocytes lacking axial elements. Mol. Biol. Cell *15*, 827–837.

Liu, L., Franco, S., Spyropoulos, B., Moens, P.B., Blasco, M.A., and Keefe, D.L. (2004). Irregular telomeres impair meiotic synapsis and recombination in mice. Proc. Natl. Acad. Sci. USA *101*, 6496–6501.

Malone, C.J., Fixsen, W.D., Horvitz, H.R., and Han, M. (1999). UNC-84 localizes to the nuclear envelope and is required for nuclear migration and anchoring during *C. elegans* development. Development *126*, 3171–3181.

Malone, C.J., Misner, L., Le Bot, N., Tsai, M.C., Campbell, J.M., Ahringer, J., and White, J.G. (2003). The *C. elegans* hook protein, ZYG-12, mediates the essential attachment between the centrosome and nucleus. Cell *115*, 825–836.

McGee, M.D., Rillo, R., Anderson, A.S., and Starr, D.A. (2006). UNC-83 is a KASH protein required for nuclear migration and is recruited to the outer nuclear membrane by a physical interaction with the SUN protein UNC-84. Mol. Biol. Cell *17*, 1790–1801.

Meuwissen, R.L., Offenberg, H.H., Dietrich, A.J., Riesewijk, A., van Iersel, M., and Heyting, C. (1992). A coiled-coil related protein specific for synapsed regions of meiotic prophase chromosomes. EMBO J. *11*, 5091–5100.

Moens, P.B., Chen, D.J., Shen, Z., Kolas, N., Tarsounas, M., Heng, H.H., and Spyropoulos, B. (1997). Rad51 immunocytology in rat and mouse spermatocytes and oocytes. Chromosoma *106*, 207–215.

Moens, P.B., Pearlman, R.E., Heng, H.H., and Traut, W. (1998). Chromosome cores and chromatin at meiotic prophase. Curr. Top. Dev. Biol. *37*, 241–262.

Moens, P.B., Kolas, N.K., Tarsounas, M., Marcon, E., Cohen, P.E., and Spyropoulos, B. (2002). The time course and chromosomal localization of recombination-related proteins at meiosis in the mouse are compatible with models that can resolve the early DNA-DNA interactions without reciprocal recombination. J. Cell Sci. *115*, 1611–1622.

Moss, S.B., Burnham, B.L., and Bellve, A.R. (1993). The differential expression of lamin epitopes during mouse spermatogenesis. Mol. Reprod. Dev. *34*, 164–174.

Padmakumar, V.C., Libotte, T., Lu, W., Zaim, H., Abraham, S., Noegel, A.A., Gotzmann, J., Foisner, R., and Karakesisoglou, I. (2005). The inner nuclear membrane protein Sun1 mediates the anchorage of Nesprin-2 to the nuclear envelope. J. Cell Sci. *118*, 3419–3430.

Roeder, G.S., and Bailis, J.M. (2000). The pachytene checkpoint. Trends Genet. *16*, 395–403.

Russell L.D., Ettlin R.A., Sinha Hikim A.P., and Clegg E.D., eds. (1990). Histological and Histopathological Evaluation of the Testis (Clearwater, FL: Cache River Press).

Scherthan, H. (2001). A bouquet makes ends meet. Nat. Rev. Mol. Cell Biol. *2*, 621–627.

Scherthan, H. (2003). Knockout mice provide novel insights into meiotic chromosome and telomere dynamics. Cytogenet. Genome Res. *103*, 235–244.

Scherthan, H. (2006). Meiotic telomeres. In Telomeres, Second Edition, T. de Lange, V. Lundblad, and E. Blackburn, eds. (Cold Spring Harbor, NY: Cold Spring Harbor Laboratory Press), pp. 225–259.

Scherthan, H., Weich, S., Schwegler, H., Heyting, C., Harle, M., and Cremer, T. (1996). Centromere and telomere movements during early meiotic prophase of mouse and man are associated with the onset of chromosome pairing. J. Cell Biol. *134*, 1109–1125.

Scherthan, H., Jerratsch, M., Li, B., Smith, S., Hulten, M., Lock, T., and de Lange, T. (2000). Mammalian meiotic telomeres: protein composition and redistribution in relation to nuclear pores. Mol. Biol. Cell *11*, 4189–4203.

Starr, D.A., and Fischer, J.A. (2005). KASH 'n Karry: the KASH domain family of cargo-specific cytoskeletal adaptor proteins. Bioessays *27*, 1136–1146.

Starr, D.A., and Han, M. (2002). Role of ANC-1 in tethering nuclei to the actin cytoskeleton. Science *298*, 406–409.

Starr, D.A., Hermann, G.J., Malone, C.J., Fixsen, W., Priess, J.R., Horvitz, H.R., and Han, M. (2001). unc-83 encodes a novel component of the nuclear envelope and is essential for proper nuclear migration. Development *128*, 5039–5050.

Tornusciolo, D.R., Schmidt, R.E., and Roth, K.A. (1995). Simultaneous detection of TDT-mediated dUTP-biotin nick end-labeling (TUNEL)-positive cells and multiple immunohistochemical markers in single tissue sections. Biotechniques *19*, 800–805.

Wu, H.Y., and Burgess, S.M. (2006). Ndj1, a telomere-associated protein, promotes meiotic recombination in budding yeast. Mol. Cell. Biol. *26*, 3683–3694.

Yu, J., Starr, D.A., Wu, X., Parkhurst, S.M., Zhuang, Y., Xu, T., Xu, R., and Han, M. (2006). The KASH domain protein MSP-300 plays an essential role in nuclear anchoring during *Drosophila* oogenesis. Dev. Biol. *289*, 336–345.

Zhang, Q., Ragnauth, C.D., Skepper, J.N., Worth, N.F., Warren, D.T., Roberts, R.G., Weissberg, P.L., Ellis, J.A., and Shanahan, C.M. (2005). Nesprin-2 is a multi-isomeric protein that binds lamin and emerin at the nuclear envelope and forms a subcellular network in skeletal muscle. J. Cell Sci. *118*, 673–687.

Zhang, X., Xu, R., Zhu, B., Yang, X., Ding, X., Duan, S., Xu, T., Zhuang, Y., and Han, M. (2007). Syne-1 and Syne-2 play crucial roles in myonuclear anchorage and motor neuron innervation. Development *134*, 901–908.

Zhen, Y.Y., Libotte, T., Munck, M., Noegel, A.A., and Korenbaum, E. (2002). NUANCE, a giant protein connecting the nucleus and actin cytoskeleton. J. Cell Sci. *115*, 3207–3222.

Zickler, D. (2006). From early homologue recognition to synaptonemal complex formation. Chromosoma *115*, 158–174.